JOURNAL OF MATERIALS SCIENCE 30 (1995) 5272–5280

Chemical states of the molybdenum disilicide ($MoSi_2$) surface

L. SHAW
Department of Metallurgy and Institute of Materials Science, University of Connecticut, Storrs, CT 06269, USA

R. ABBASCHIAN
Department of Materials Science and Engineering, University of Florida, Gainesville, FL 32611, USA

The analysis of the oxidation of $MoSi_2$ at room temperature was carried out using X-ray photoelectron spectroscopy. A clean surface of $MoSi_2$ was obtained by sputter-etching the bulk material inside the spectrometer, and the chemical states of the surface were examined with both high and low take-off angles for the conditions of as-etched and exposed to the air for different times. The commercially pure $MoSi_2$ powder was also investigated in the as-received condition. The analysis indicated that the exposure of a clean molybdenum disilicide to the air for just a few minutes led to the formation of SiO_2 and MoO_2, and this oxidation would persist at least for more than 24 h with the final surface of $MoSi_2$ being covered by a duplex oxide layer of $SiO_2 + MoO_3$.

1. Introduction

Molybdenum disilicide ($MoSi_2$) is a potentially useful high-temperature matrix for advanced structural composites because it has a high melting point (2020 °C), excellent resistance to oxidation and hot corrosion, and a moderate density (6.26 g cm^{-3}). However, like other intermetallics, the use of $MoSi_2$ as a structural material is impeded by its low ambient-temperature fracture toughness and poor elevated-temperature strength. Consequently, current work on $MoSi_2$ emphasizes simultaneous improvement of the low-temperature ductility and high-temperature strength. Improvement in low-temperature toughness has been achieved by the incorporation of ductile refractory metals, such as niobium [1–9], partially stabilized zirconia [10, 11], silicon carbide whiskers [12–16], and by novel processing techniques such as *in situ* formation of SiC-reinforced composites using a solid-state displacement reaction [17–19]. Improved high-temperature strength, toughness and creep resistance have been observed with the addition of silicon carbide whiskers [13–15], the *in situ* formation of silicon carbide by solid-state displacement reaction [17–19] or by the XD™ process [20], and the addition of elemental carbon during consolidation [21].

One prominent feature of the processing and properties of $MoSi_2$ is the presence of silica in the $MoSi_2$ matrix. It has been established that SiO_2 normally exhibits a non-wetting behaviour in $MoSi_2$ and thus segregates to the grain boundaries and triple points as spheroidal particles [21–24]. SiO_2 is expected to be detrimental to the mechanical properties of $MoSi_2$, because it may serve as crack-nucleation sites at low temperature, while it may enhance grain-boundary sliding and diffusion above its softening point ($\sim$1200 °C). Numerous studies have shown that this is, indeed, the case. An example was provided by Maxwell [25] who intentionally added carbon (deoxidant) to $MoSi_2$ and found that $MoSi_2$ had better creep resistance and lower high-temperature plasticity than the counterpart without carbon addition. Maloy *et al.* [21] also showed the improvement in high-temperature hardness and toughness by the carbon addition, and attributed this to the removal of a glassy SiO_2 second-phase in the $MoSi_2$ matrix and the formation of SiC and $Mo_{\leq 5}Si_3C_{\leq 1}$. Similar results were also obtained by Aikin [26] who demonstrated that ultra-pure $MoSi_2$ with a very low oxygen content (and low silica) did not exhibit plasticity below 1400 °C. SiO_2 has also been reported to be responsible for the degradation of the diffusion barrier coatings at the fibre/matrix interface in ductile fibre-reinforced $MoSi_2$ [27].

SiO_2 in the consolidated $MoSi_2$ is considered to come from a protective amorphous layer on the surface of $MoSi_2$ powder before consolidation [21, 22, 24, 28]. This amorphous silica layer has been reported to be preferentially formed above 500 °C, while below that temperature a duplex oxide layer containing silica and molybdenum oxide will form [29, 30]. However, whether or not the oxidation occurs at room temperature has never been reported. Nevertheless, a study conducted by Schwarz *et al.* [24] found the presence of SiO_2 in the mechanically alloyed $MoSi_2$ fabricated from silicon chunks and inside an argon-filled glovebox. The $MoSi_2$ powder was only

0022–2461

exposed to the air for a very short time during the loading of the hot-press dies into the induction furnace. This result clearly indicated that oxygen was very easily picked up by $MoSi_2$ powder even at room temperature, implying that the oxidation of $MoSi_2$ might also occur at room temperature.

The above discussion clearly shows that properties of $MoSi_2$ are related to the presence of SiO_2. In addition, processing of $MoSi_2$ composites often relies on the chemical states of the surface of the $MoSi_2$ powder. For example, the chemical information from the $MoSi_2$ surface was utilized to co-disperse $MoSi_2$ powder and SiC whiskers in a tape-casting slip for fabricating SiC whisker-reinforced composites [16]. Thus, information about the formation of the protective oxide layers on $MoSi_2$ is very useful in the prediction and control of the presence of SiO_2, as well as in the processing of $MoSi_2$ and its composites. However, as discussed above, there is incomplete information about the oxidation at room temperature. Therefore, the present work intended to study the formation of oxide layers on the surface of $MoSi_2$ at room temperatures using X-ray photoelectron spectroscopy (XPS or ESCA). Spectra obtained from ESCA correspond to the chemical states of a solid surface up to a depth of a few nanometres. Thus, ESCA is a suitable tool for the investigation of oxidation at the very early stage, or at room temperature at which oxidation may or may not proceed.

2. Experimental procedure

Commercially pure $MoSi_2$ powder was supplied by Johnson Mathey Incorporation and prepared through a proprietary fusion process, followed by milling and grinding at ambient temperatures to obtain the product size of -325 mesh. The median Stokes diameter of the as-received powder was determined to be 1.12 μm by centrifugal photosedimentation. The composition reported by the vendor was Mo > 61.0%, Si 36.6%, C 0.06%, N 0.03%, O 1.22% and metallic impurities < 0.5% (wt %). X-ray diffraction (XRD) analysis showed only $MoSi_2$ peaks (CuK_α radiation, 2θ angles from 5°–100°), indicating other phases, if present, were below the volume fraction detectable by XRD or were amorphous, such as amorphous SiO_2 thin films on the surface of $MoSi_2$ powder.

The samples used for the ESCA analysis were in powder form (the as-received condition) as well as in consolidated form. The consolidation was carried out by hot pressing the commercially pure $MoSi_2$ powder at 1400 °C for 60 min under a pressure of 40 MPa. The samples with dimensions of $15 \times 10 \times 2$ mm were cut from the hot-pressed discs using a diamond wafering blade, finish polished with 0.25 μm diamond paste, and finally cleaned in acetone and then methanol before analysis.

X-ray photoelectron spectra of the hot-pressed samples were obtained with a PHI 5100 ESCA system using a MgK_α source (1253.6 eV) with a power of 300 W. A pass energy of 35.75 eV was used for detailed scans, while 89.45 eV was utilized for all survey spectra. The scan steps were 0.1 eV for detailed scans and 1.0 eV for survey. Two take-off angles, 45° and 15°, were used for the analysis to differentiate the signals from the surface and bulk, because a spectrum from a high take-off angle maximizes the signal from the bulk relative to that from the surface layer, while a spectrum from a low take-off angle enhances the signal from the surface. The spectra of the adventitious hydrocarbon (C 1s at 285.0 eV) were taken as references for charge correction. The survey and high-energy resolution spectra of the C 1s, O 1s, Si 2p, and Mo 3d levels were obtained under a vacuum of 1.4×10^{-10} torr (1 torr = 133.322 Pa) for the conditions of as-polished, sputter-etched, and exposed to the air for different times after the sputter-etching. Sputter-etching was carried out using an argon-ion gun with a voltage of 4 kV, resulting in an approximate rate of sputtered-away thickness of 1 nm min^{-1}. Three sputtered-away thicknesses (50, 100 and 200 nm) and two exposure times (5 min and 24 h after 200 nm was sputtered-away) were analysed.

XPS analysis of the as-received powder was conducted with a XASM 800 analyser using a MgK_α source with a power of 240 W. A take-off angle of 45° was used for all the analysis. A scan step of 0.05 eV was utilized for detailed scans and 0.3 eV for survey. The spectra were obtained under a vacuum of 1.0×10^{-8} torr with the powder pressed on a double sided tape. Again, C 1s of 285.0 eV was taken as reference for charge correction.

3. Results and discussion

3.1. Survey spectra of the consolidated $MoSi_2$

In order to determine whether or not oxidation proceeds at ambient temperatures, a fresh surface of $MoSi_2$ was formed inside the chamber of the spectrometer by sputter-etching the as-polished sample. It was found that survey spectra for three sputter-etched conditions (with 50, 100 and 200 nm sputtered away) were the same, while they were different from the spectrum for the as-polished condition. The as-polished sample exhibited a higher oxygen peak and lower molybdenum and silicon peaks than the sputter-etched samples, indicating that either some oxygen absorbed on the surface of the as-polished sample or a thin oxide layer was formed at ambient temperatures after the polishing. Regardless of what it was, this layer was thinner than 50 nm because the spectra for the samples with 50, 100 and 200 nm sputtered away were the same.

The survey spectrum for the sample with 200 nm sputtered away is shown in Fig. 1a. As seen in the figure, the oxygen peak is very low and there is almost no carbon peak at this condition. The spectrum of this sample after exposure to the air for 5 min is presented in Fig. 1b for comparison. The apparent differences between these two conditions are the increase of the oxygen signal and the introduction of carbon by the exposure. The survey spectrum for the sample exposed to the air for 24 h exhibited similar characteristics to the sample exposed to the air for 5 min.

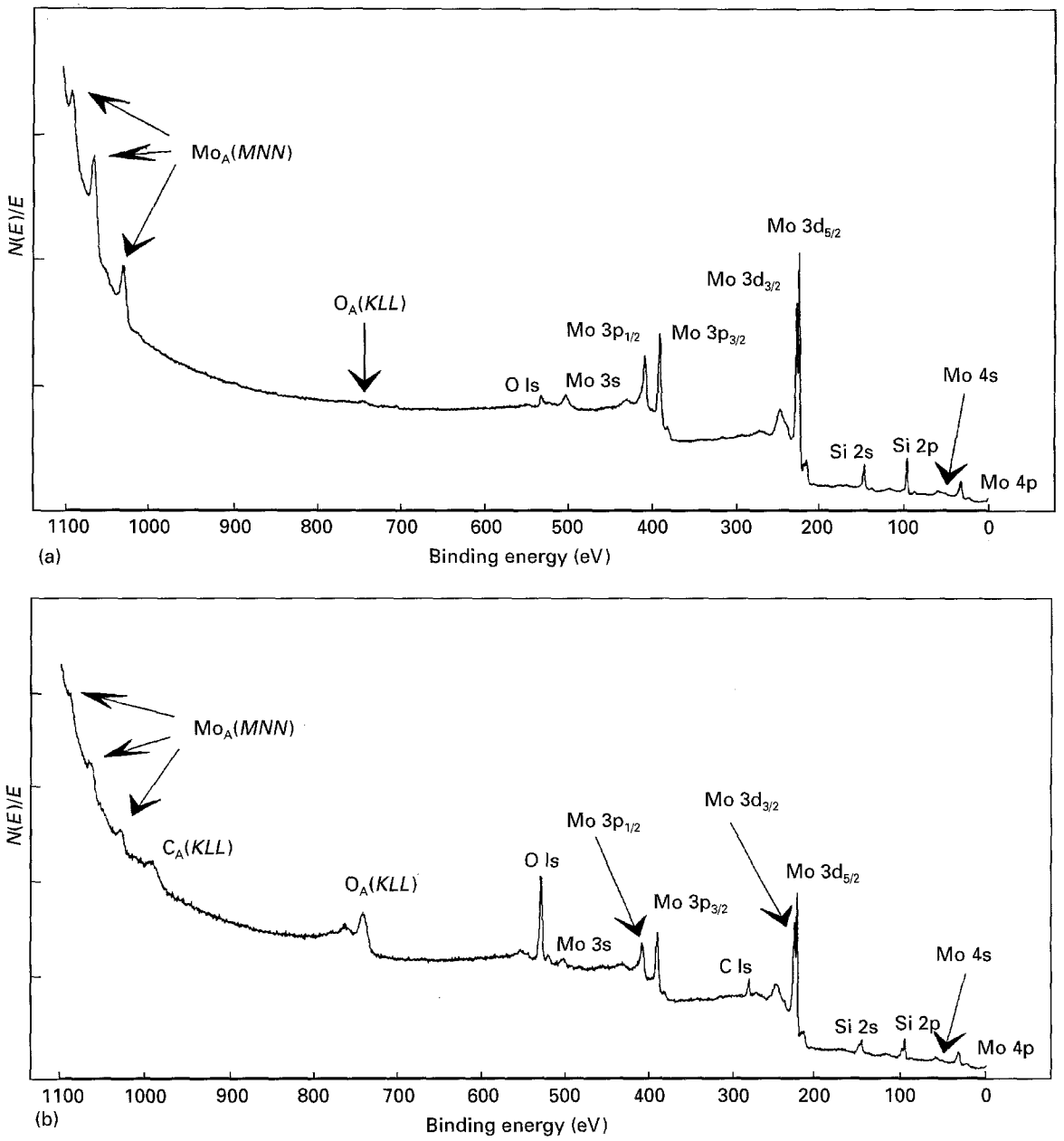

Figure 1 Survey spectra of the consolidated $MoSi_2$. Subscript A indicates the Auger line. (a) Sputter-etched in the spectrometer with 200 nm sputtered away, and (b) exposed to the air for 5 min after the sputter-etching.

3.2. High-energy resolution scans of the consolidated $MoSi_2$

Corresponding to the change of the survey spectra, the high-energy resolution scans also displayed salient changes. The spectra of the Si 2p, Mo 3d and O 1s for the samples under different conditions are shown in Figs 2–4, respectively. To facilitate the discussion of the current results, the binding energies of the Si 2p, Mo 3d and O 1s measured from pure compounds by other investigators [31–44] are listed in Table I. For convenience of observation, the binding energy for each element chosen from the other studies is also marked in the figures. Comparison between the current spectra and the table clearly indicates that the peak positions of the Si 2p and Mo 3d fall into the ranges reported by the other investigators. As such, the selection of the binding energies marked in the figures is simply for the purpose of making the binding-energy points in the figures fit the spectra as well as possible.

Fig. 2 illustrates the evolution of the Si 2p spectrum with exposure time. At the sputter-etching condition (200 nm sputtered away) and 45° take-off angle (Fig. 2a), only one symmetrical Si 2p peak appeared which corresponded to the silicon in $MoSi_2$. After exposure to the air for 5 min (Fig. 2c), another Si 2p peak emerged which corresponded to the silicon in SiO_2. As the exposure time was extended to 24 h (Fig. 2e), the Si 2p peak from SiO_2 increased in intensity while the intensity of the Si 2p peak from $MoSi_2$ decreased, indicating the increase of SiO_2 formed on the surface of $MoSi_2$. Comparison of the spectra of high and low take-off angles reveals two more features: (1) SiO_2 resides on the very surface of $MoSi_2$ because the intensities of the Si 2p for SiO_2 in Fig. 2d and f are much higher than those in Fig. 2c and e; and (2) a clean surface with no silica is obtained with the present sputter-etching process, as indicated by Fig. 2a and b. Because the spectra of the Si 2p for the three sputter-etching conditions (with 50, 100 and

TABLE I Binding energies of SiO_2, $MoSi_2$, MoO_3, MoO_2 free H_2O and O_2 as given in the literature

Compound	Binding energy (eV)				Reference
	O 1s	Si 2p	Mo 3d5	Mo 3d3	
SiO_2 (crystal)	532.6	103.4			[31]
	534.3	NA			[32]
	532.7	103.5			[33]
	NA	103.2			[34]
SiO_2 (quartz)	532.5	103.5			[35]
	NA	103.0			[36]
SiO_2 (cristobalite)	532.3[a]	103.2[a]			[35]
SiO_2 (gel)	530.6	101.2			[37]
	532.7	103.4			[35]
	533.2	104.1			[38]
$MoSi_2$		99.36[a]	227.68[a]	230.88[a]	[35]
		99.10	227.4	NA	[39]
MoO_3	530.3		232.5	235.7	[40]
	529.9		232.2	NA	[41]
	531.1[a]		232.5[a]	235.6[a]	[42]
	530.1		231.1	NA	[37]
	531.1		NA	NA	[43]
MoO_2	529.6		228.8	NA	[41]
	530.4		229.1	232.3	[40]
	530.8[a]		229.4[a]	232.5[a]	[42]
O_2 (gas)	543.1				[44]
H_2O (gas)	539.7				[44]

[a] The binding energies marked in Figs 2–5.

200 nm sputtered away) were the same, it could be concluded that a clean surface free from oxides could be attained by sputtering away 50 nm thickness.

Evolution of the Mo 3d peak with exposure to the air is presented in Fig. 3. At the sputter-etching condition (Fig. 3a and b), no molybdenum oxide existed on the surface of $MoSi_2$, as indicated by the presence of only a pair of Mo 3d peaks which came from molybdenum in $MoSi_2$. Exposure to the air for 5 min caused the formation of tiny amounts of MoO_2 on the surface of $MoSi_2$, as indicated by the asymmetry of the Mo $3d_{5/2}$ peak in both Fig. 3c and d, and the asymmetry of the Mo $3d_{3/2}$ peak in Fig. 3d. However, it is quite clear that there was no MoO_3 formation at this stage because no Mo 3d peak appeared at the position of the binding energy corresponding to MoO_3. When the exposure to air was extended to 24 h, though (Fig. 3e and f), a new pair of Mo 3d peaks appeared which was identified as being from the molybdenum in MoO_3. When take-off angle was high (Fig. 3e), the Mo 3d peaks from MoO_3 was very weak. But they become obvious when the take-off angle was low (Fig. 3f), clearly indicating the presence of MoO_3 actually on the surface of $MoSi_2$.

The apparent asymmetries of the O 1s peaks in Fig. 4 indicate the presence of several oxygen species with different binding energies. The O 1s peaks were very weak at the sputter-etched condition (Fig. 4a and b), as compared to the exposed conditions. Obviously, the O 1s peaks from SiO_2, MoO_3, MoO_2, free oxygen and water (see Table I) could not explain the shape of the current O 1s lines in Fig. 4. The main discrepancy is at the high binding energy region (above $\sim$533 eV) where no reasonable O 1s peaks from the literature could be found. It is well known that Fig. 4a, a spectrum from a high take-off angle, maximized the signal from the bulk relative to that from the surface layer, while Fig. 4b, a spectrum from a low take-off angle, enhanced the signal from the surface. Thus, the O 1s signal in the high binding energy region probably comes from the interstitial oxygen in $MoSi_2$. The O 1s signal in the low binding energy region (from 533–529 eV) corresponded to the binding energy of SiO_2, MoO_2 and MoO_3, as shown in Fig. 4b–f. In combination with Figs 2 and 3, it could be deduced that for the 5 min exposure, both SiO_2 and MoO_2 were formed with the domination of SiO_2 phase. When the exposure was extended to 24 h, the MoO_2 converted to MoO_3 and the resultant oxide layer consisted of SiO_2 and MoO_3. In Fig. 4b, a spectrum at the sputter-etched condition, a weak O 1s peak also appeared at the position corresponding to the binding energy of SiO_2, MoO_2 and MoO_3. However, at this condition the spectra of the Si 2p and Mo 3d clearly exhibited no oxides, as discussed above. Thus, the O 1s signal in this case probably came from the absorbed oxygen.

From the above discussion, it can be summarized that 5 min exposure of the clean $MoSi_2$ surface to the air leads to the formation of SiO_2 and tiny amounts of MoO_2, and that after 24 h exposure, SiO_2 is further increased while MoO_2 converted to MoO_3, leading to a duplex oxide layer of $SiO_2 + MoO_3$.

3.3. Oxidation mechanisms

The oxidation of $MoSi_2$ may be carried out in several intermediate steps. As shown in Equations 1–5, $MoSi_2$ may dissociate step by step to form SiO_2 and lower silicon content phases, and eventually end up with the oxidation of molybdenum.

$$5/7MoSi_2 + O_2 = SiO_2 + 1/7Mo_5Si_3 \quad (1)$$

$$3/4Mo_5Si_3 + O_2 = SiO_2 + 5/4Mo_3Si \quad (2)$$

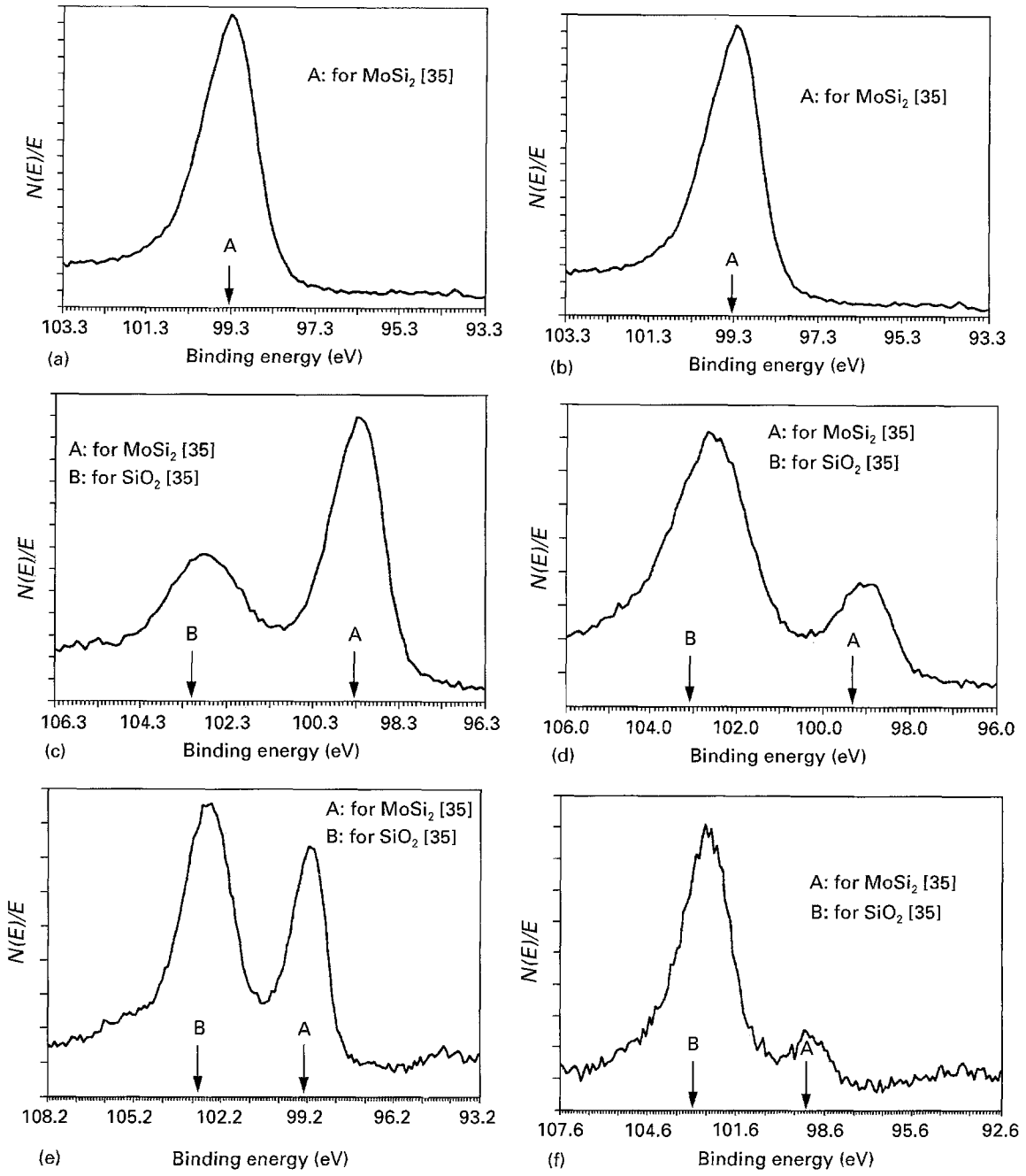

Figure 2 Spectra of the Si 2p for the consolidated $MoSi_2$ with a take-off angle of 45° for (a), (c) and (e), and 15° for (b), (d) and (f). (a, b) sputter-etched in the spectrometer with 200 nm sputtered away; (c, d) exposed to the air for 5 min; and (e, f) exposed to the air for 24 h.

$$Mo_3Si + O_2 = SiO_2 + 3Mo \quad (3)$$

$$Mo + O_2 = MoO_2 \quad (4)$$

$$2MoO_2 + O_2 = 2MoO_3 \quad (5)$$

Thermodynamic calculation of the free energy changes for these reactions (Table II) shows that all these reactions are thermodynamically possible. In fact, based on the silicon dissociation pressure for the various silicide phases, the free energies of formation of SiO_2, the free energies of vaporization of silicon, and the free energies of formation of MoO_2 and MoO_3, Bartlett *et al.* [29] have proposed a diagram showing the stability zone of condensed phases in the $MoSi_2$–O_2 system. The diagram shows that the dissociation and oxidation of $MoSi_2$ pursue the following route with the increase of oxygen pressure from 10^{-28} to 10^{-4} atm

$$MoSi_2 \rightarrow SiO_2 + Mo_5Si_3 \rightarrow SiO_2 + Mo \rightarrow SiO_2 + MoO_2 \rightarrow SiO_2 + MoO_3 \quad (6)$$

This route is very similar to the sequence shown in Equations 1–5 except no Mo_3Si is formed. However, when the oxygen pressure is high and therefore the driving force for the oxidation is large, this reaction sequence may not be right. The current XPS analyses seem to display another reaction route, that is, silicon and molybdenum oxides form directly from $MoSi_2$, as shown in Equation 7. Then, MoO_3 forms from the further oxidation of MoO_2 (Equation 5). Because no XPS spectra data are available for Mo_5Si_3 and Mo_3Si,

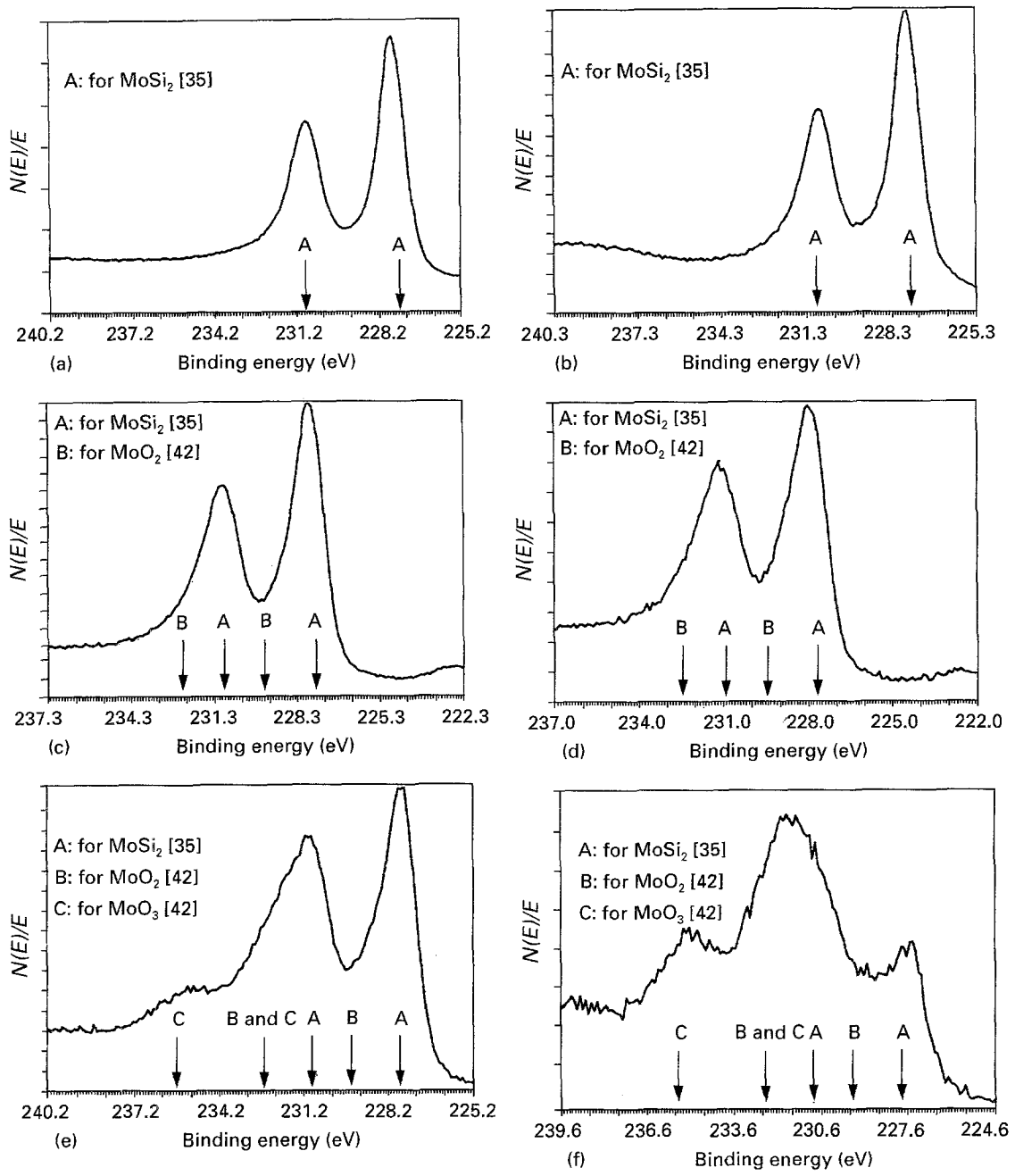

Figure 3 Spectra of the Mo $3d_{5/2}$ and Mo $3d_{3/2}$ for the consolidated $MoSi_2$. The conditions for (a)–(f) are the same as those in Fig. 2.

we still cannot rule out the possibility of the reaction sequence shown in Equations 1–5. However, if the oxidation proceeds as shown by Equations 1–5, it must occur very quickly because the 5 min exposure to air has already led to the formation of MoO_2

$$1/3MoSi_2 + O_2 = 2/3SiO_2 + 1/3MoO_2 \quad (7)$$

3.4. XPS analysis of the as-received powder

Because the as-received $MoSi_2$ powder is produced at the final stage by milling at room temperature, it is reasonable to compare the X-ray photoelectron spectra from the powder with those from the consolidated samples. The main difference between these two type of the sample is the exposure time of the $MoSi_2$ surface to the air, with the powder being exposed much longer than the consolidated samples. Details of the Mo 3d, O 1s and Si 2p spectra measured from the as-received $MoSi_2$ powder with a take-off angle of 45° are shown in Fig. 5. It is noted from Fig. 5a that the Mo 3d from MoO_3 predominates the spectra of the as-received powder, in contrast to the domination of the Mo 3d from $MoSi_2$ (Fig. 3e) for the consolidated sample with sputter-etching followed by 24 h exposure to the air. This result indicates that at room temperature the oxidation of $MoSi_2$ still advances slowly even after exposure to the air for 24 h, and finally the surface of $MoSi_2$ is covered with a duplex oxide layer of $SiO_2 + MoO_3$. The increase of MoO_3 on the surface of $MoSi_2$ after the 24 h exposure to the air is also substantiated by examination of the O 1s spectra. Comparison of Figs 4e and 5b shows that the relative intensity of the O 1s from MoO_3 with respect to the peak of the O 1s from SiO_2 has increased from the 24 h exposure condition to the

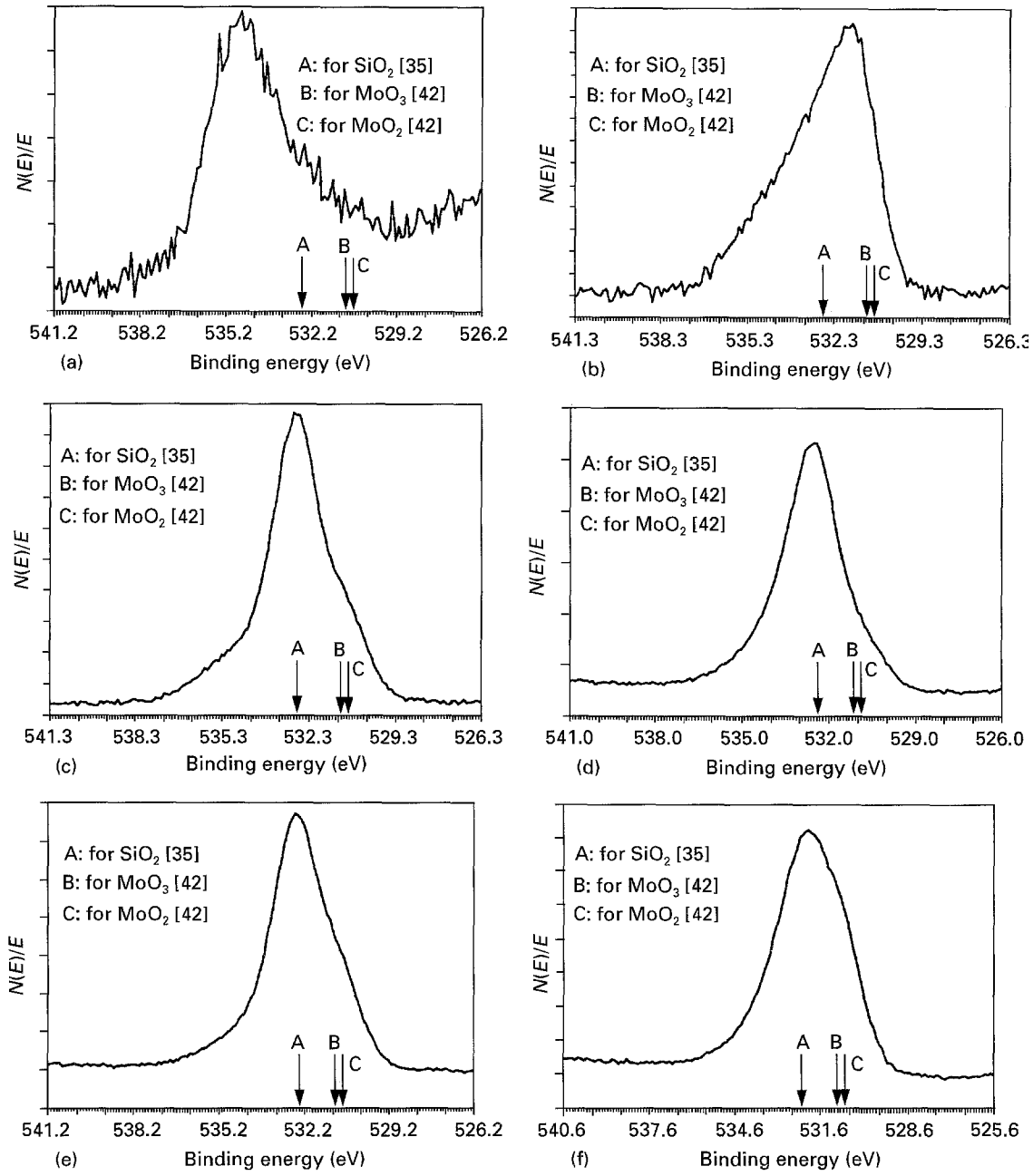

Figure 4 Spectra of the O 1s for the consolidated $MoSi_2$. The conditions for (a)–(f) are the same as those in Fig. 2.

TABLE II The standard free energy changes of some possible reactions for the oxidation of $MoSi_2$ [45]

Reaction	Free energy change, $\Delta G_{298\,K}$ (kcal mol^{-1})
1	− 192.47
2	− 183.22
3	− 176.31
4	− 127.41
5	− 64.57
6	− 168.17

powder form. In contrast, the relative intensities of the Si 2p from $MoSi_2$ and SiO_2 for the 24 h exposure condition (Fig. 2e) and powder form (Fig. 5c) are similar, suggesting that the SiO_2 formation is completed at or before 24 h exposure to the air. In short, the comparison of the Mo 3d, O 1s and Si 2p spectra between the 24 h exposure condition and powder form, reveals that the formation of SiO_2 on the surface of $MoSi_2$ proceeds very quickly and is completed at or before 24 h exposure to the air, while the formation of MoO_3 lasts for more than 24 h at ambient temperatures.

4. Conclusions

The analysis of the oxidation of $MoSi_2$ at room temperature has been carried out using X-ray photoelectron spectroscopy. According to the XPS analysis of the consolidated $MoSi_2$ and commercially pure $MoSi_2$ powder, the following conclusions can be drawn.

1. Oxidation of $MoSi_2$ proceeds at room temperature with a very fast rate in the sense that exposure of clean molybdenum disilicide to the air for a very short time (of the order of minutes) leads to the formation of SiO_2 and MoO_2.

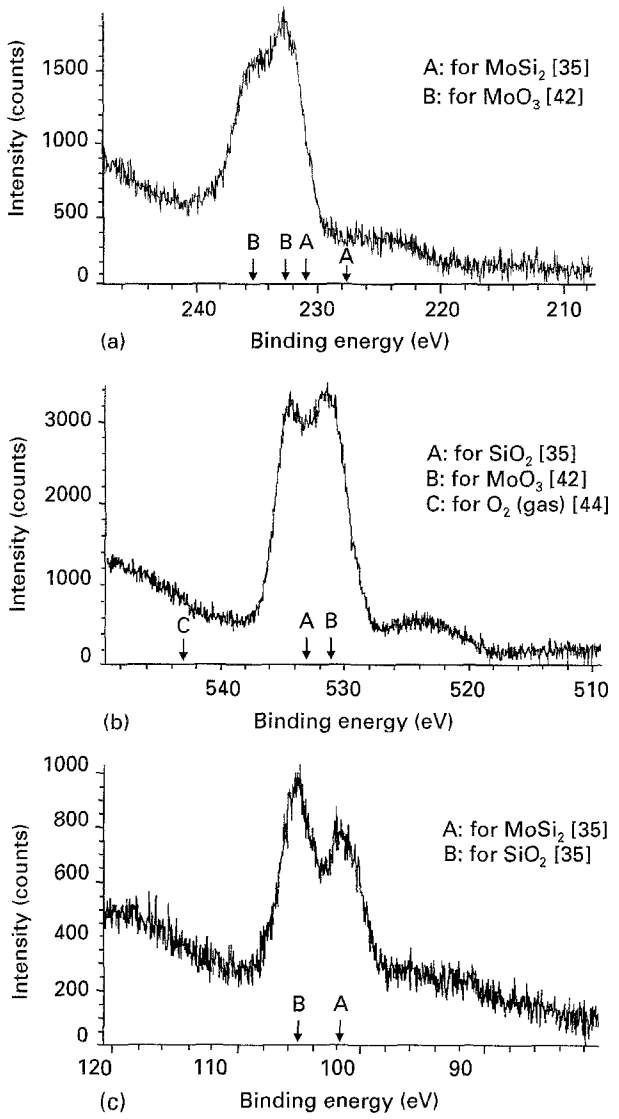

Figure 5 Spectra from the commercially pure $MoSi_2$ powder with a take-off angle of 45° (a) Mo $3d_{5/2}$ and Mo $3d_{3/2}$; (b) O 1s; and (c) Si 2p spectrum.

2. The most possible reaction sequence for the oxidation of $MoSi_2$ at ambient temperature is $MoSi_2 \rightarrow SiO_2 + MoO_2 \rightarrow SiO_2 + MoO_3$.

3. The oxidation at ambient temperature lasts for at least 24 h with the final surface of $MoSi_2$ being covered by a duplex oxide layer of $SiO_2 + MoO_3$.

Acknowledgements

The authors are grateful for the support of the Defense Advanced Research Projects Agency (DARPA) and Office of Naval Research through grant N00014-91-J-4075.

References

1. E. FITZER, in "Whisker- and fiber-toughened ceramics", edited by R. A. Bradley, D. E. Clark, D. C. Larsen and J. O. Stiegler (ASM International, Materials Park, OH, 1988) pp. 165–92.
2. T. C. LU, A. G. EVANS, R. J. HECHT and R. MEHRABIAN, *Acta Metall. Mater.* **39** (1991) 1853.
3. L. XIAO, Y. S. KIM, R. ABBASCHIAN and R. J. HECHT, *Mater. Sci. Eng.* **A144** (1991) 277.
4. L. XIAO and R. ABBASCHIAN, *Metall. Trans.* **23A** (1992) 2863.
5. *Idem, Mater. Sci. Eng.* **A155** (1992) 135.
6. *Idem*, in "Advanced metal matrix composites for elevated temperatures", edited by M. N. Goungor, E. J. Lavernia and S. G. Fishman (ASM International, Materials Park, OH, 1991) pp. 21–31.
7. L. XIAO, Y. S. KIM and R. ABBASCHIAN, in "Intermetallic matrix composites", Proceedings of MRS Symposium, vol. 194, edited by D. L. Anton, P. L. Martin, D. B. Miracle and R. McMeeking (Materials Research Society, Pittsburgh, PA, 1990) pp. 399–404.
8. L. XIAO and R. ABBASCHIAN, *Metall. Trans.* **24A** (1993) 403.
9. L. SHAW and R. ABBASCHIAN, *Acta Metall. Mater.* **42** (1994) 213.
10. J. J. PETROVIC and R. E. HONNELL, *J. Mater. Sci.* **25** (1990) 4453.
11. J. J. PETROVIC, R. E. HONNELL, T. E. MITCHELL, R. K. WADE and K. J. McCLELLAN, *Ceram. Eng. Sci. Proc.* **12** (1991) 1633.
12. F. D. GAC and J. J. PETROVIC, *J. Am. Ceram. Soc.* **68** (1985) C-200.
13. W. S. GIBBS, J. J. PETROVIC and R. E. HONNELL, *Ceram. Eng. Sci. Proc.* **8** (1987) 645.
14. D. H. CARTER, J. J. PETROVIC, R. E. HONNELL and W. S. GIBBS, *ibid.* **10** (1989) 1121.
15. K. SADANANDA, H. JONES, J. FENG, J. J. PETROVIC and A. K. VASUDEVAN, *Ceram. Eng. Sci. Proc.* **12** (1991) 1671.
16. L. XIAO and R. ABBASCHIAN, *J. Am. Ceram. Soc.*, submitted.
17. C. H. HENAGER Jr, J. L. BRIMHALL, J. S. VETRANO and J. P. HIRTH, in "Intermetallic matrix composites II", Proceedings of MRS Symposium, vol. 273, edited by D. Miracle, J. Graves and D. Anton (Materials Research Society, Pittsburgh, PA, 1992) pp. 281–7.
18. C. H. HENAGER Jr, J. L. BRIMHALL and J. P. HIRTH, in "Synthesis and processing of ceramics: scientific issues", Proceedings of MRS Symposium, vol. 249, edited by W. E. Rhine, T. M. Shaw, R. J. Gottschall and Y. Chen (Materials Research Society, Pittsburgh, PA, 1992) pp. 523–8.
19. *Idem, Mater. Sci. Eng.* **A155** (1992) 109.
20. R. M. AIKIN Jr, *Ceram. Eng. Sci. Proc.* **12** (1991) 1643.
21. S. MALOY, A. H. HEUER, J. LEWANDOWSKI and J. PETROVIC, *J. Am. Ceram. Soc.* **74** (1991) 2704.
22. J. D. COTTON, Y. S. KIM and M. J. KAUFMAN, *Mater. Sci. Eng.* **A144** (1991) 287.
23. J. P. A. LOFVANDER, J. Y. YANG, C. G. LEVI and R. MEHRABIAN, in "Advanced metal matrix composites for elevated temperatures", edited by M. N. Goungor, E. J. Lavernia and S. G. Fishman (ASM International, Materials Park, OH, 1991) pp. 1–10.
24. R. B. SCHWARZ, D. R. SRINIVASAN, J. J. PETROVIC and C. J. MAGGIORE, *Mater. Sci. Eng.* **A155** (1992) 75.
25. W. A. MAXWELL, National Advisory Committee for Aeronautics, Report E52B06 (1952).
26. R. M. AIKIN Jr, *Scripta Metall. Mater.* **26** (1992) 1025.
27. L. SHAW and R. ABBASCHIAN, *J. Am. Ceram. Soc.* **76** (1993) 2305.
28. S. JAYASHANKAR and M. J. KAUFMAN, *J. Mater. Res.* **8** (1993) 1428.
29. R. W. BARTLETT, J. W. McCAMONT and P. R. GAGE, *J. Am. Ceram. Soc.* **48** (1965) 551.
30. P. J. MESCHTER, *Metall. Trans.* **23A** (1992) 1763.
31. T. L. BARR, *Appl. Surf. Sci.* **15** (1983).
32. K. KISHI and S. IKEDA, *Bull. Chem. Soc. Jpn* **46** (1973) 341.
33. V. I. NEFEDOV, Y. V. SALYN, G. LEONHAVDT and R. SCHEIBE, *J. Electron Spectrosc. Relat. Phenom.* **10** (1977) 121.
34. M. KLASSON, A. BERNDTSSON, J. HEDMAN, R. NILSSON, R. NYHOLM and C. NORDLING, *ibid.* **3** (1974) 427.
35. C. D. WAGNER, D. E. PASSOJA, H. F. HILLERY, T. G. KINISKY, H. A. SIX, W. T. JANSEN and J. A. TAYLOR, *J. Vac. Sci. Technol.* **21** (1982) 933.

36. J. W. ROBINSON, "Practical handbook of spectroscopy" (CRC Press, 1991) p. 394.
37. P. GAJARDO, D. PIROTTE, C. DEFOSSE, P. GRANGE and B. DELMON, *J. Electron Spectrosc. Relat. Phenom.* **17** (1979) 121.
38. F. P. J. KERKHOF, J. A. MONLIJN and A. HEERES, *ibid.* **14** (1978) 453.
39. W. A. BRAINARD and D. R. WHEELER, *J. Vac. Sci. Technol.* **15** (1978) 1800.
40. R. J. COTTON, A. M. GUZMAN and J. W. RABALAIS, *J. Appl. Phys.* **49** (1978) 409.
41. D. D. SARMA and C. N. R. RAO, *J. Electron Spectrosc. Relat. Phenom.* **20** (1980) 25.
42. T. A. PATTERSON, J. C. CARVER, D. E. LEYDEN and D. M. HERCULES, *J. Phys. Chem.* **80** (1976) 1700.
43. V. I. NEFEDOV, M. N. FIRSOV and I. S. SHAPLYGIN, *J. Electron Spectosc. Relat. Phenom.* **26** (1982) 65.
44. K. SIEGBAHN, C. NORDLING, G. JOHANSSON, J. HEDMAN, P. F. HEDEN, K. HAMRIN, U. GELIUS, T. BERGMARK, L. O. WRME, R. MANNE and Y. BAER, "ESCA applied to free molecules" (North-Holland, Amsterdam, 1971) pp. 69–73.
45. I. BARIN, O. KNACKE and O. KUBASCHEWSKI, "Thermochemical properties of inorganic substances" (Springer, Berlin, 1977).

Received 11 April 1994
and accepted 28 April 1995